

# Hybrid Quantum Annealing via Molecular Dynamics

Hiroataka Irie,<sup>\*,a,b</sup> Haozhao Liang,<sup>†,c,d</sup> Takumi Doi,<sup>‡,b,c</sup> Shinya Gongyo,<sup>§,c</sup>  
and Tetsuo Hatsuda<sup>¶,b</sup>

*AI R&I Division, Advanced Research and Innovation Center,  
DENSO CORPORATION, Global R & D Tokyo, Tokyo 108-0075, Japan<sup>a</sup>  
RIKEN Interdisciplinary Theoretical and mathematical Sciences Program  
(iTHEMS), Saitama 351-0198, Japan<sup>b</sup>  
RIKEN Nishina Center (RNC), Saitama 351-0198, Japan<sup>c</sup>  
Department of Physics, Graduate School of Science,  
The University of Tokyo, Tokyo 113-0033, Japan<sup>d</sup>*

## Abstract

A novel quantum-classical hybrid scheme is proposed to efficiently solve large-scale combinatorial optimization problems. The key concept is to introduce a Hamiltonian dynamics of the classical flux variables associated with the quantum spins of the transverse-field Ising model. Molecular dynamics of the classical fluxes can be used as a powerful preconditioner to sort out the frozen and ambivalent spins for quantum annealers. The performance and accuracy of our smooth hybridization in comparison to the standard classical algorithms (the tabu search and the simulated annealing) are demonstrated by employing the MAX-CUT and Ising spin-glass problems.

---

\*hirotaka.irie.j3a@jp.denso.com

†haozhao.liang@riken.jp

‡doi@ribf.riken.jp

§shinya.gongyo@riken.jp

¶thatsuda@riken.jp

## Introduction

Combinatorial optimizations are ubiquitous and generally represented by the Ising spin-glass model, which is computationally classified as an NP-hard problem [1]. The quantum annealing with a transverse-field Ising model [2,3] as well as the adiabatic quantum computation [4,5] provide metaheuristic quantum algorithms for such difficult combinatorial optimizations. They utilize adiabatic evolution of quantum bits (qubits) to find the ground state of Ising spin-glass models. Since quantum-annealing processors (quantum annealers) have become available [6], practical usage as well as fundamental researches on quantum optimization has largely been developed in recent years (see e.g. [7,8] and references therein).

Despite the great progress that has been taken place in the development of quantum optimization, the number of qubits as well as the noise control are still limited. To utilize such noisy intermediate-scale quantum (NISQ) devices [9], hybrid systems that are capable of dealing with large-scale optimization problems while using relatively small quantum optimization need to be developed. So far, several hybrid algorithms have been proposed in the literature (see, e.g. [10–16] and references therein). Most of them are based on the idea of decomposing original large-scale problem into subproblems to be treated by available quantum devices, so that multiple iterations between classical and quantum solvers are required to achieve high accuracy.

In this paper, we propose a novel hybrid system of quantum optimization, Hybrid Quantum Annealing (HQA), which is based on a combination of the molecular dynamics (MD) and the quantum annealing (QA). The concept of HQA is illustrated in Fig. 1. Consider the Ising spin-glass with  $N$  number of sites. The classical MD solver with continuous flux variables is suitable for identifying a set of spin configurations with low energies indicated schematically by  $A$  in the full  $2^N$ -dimensional space. Once  $A$  is identified, the quantum solver with quantum spin variables can resolve the fine structure of the reduced  $2^n$ -dimensional subspace ( $2^n \ll 2^N$ ) around  $A$  to find the minimum  $B$ . Thus, the classical solver plays a role of a preconditioner for the quantum annealer to search through the huge energy landscape effectively.

For HQA to work in practice, it is crucial to develop suitable classical Hamiltonian. We introduce such a Hamiltonian dynamics of the classical flux variables associated with the quantum spins of the transverse-field Ising Hamiltonian. Then the molecular dynamics of the classical fluxes can be used as a powerful preconditioner to sort out the frozen and ambivalent spins for quantum annealers. Since both classical and quantum Hamiltonians have the same roots, various intriguing features of QA can be imported into HQA, so that it constitutes a seamless scheme for quantum-classical hybridization. We note that the classical part of our HQA has some similarity with SVMC (Spin-vector Monte Carlo) [17], CIM (coherent Ising machine) [18] and SBM (simulated bifurcation machine) [19]. However, they are purely classical and do not contain the idea of quantum-classical hybridization.

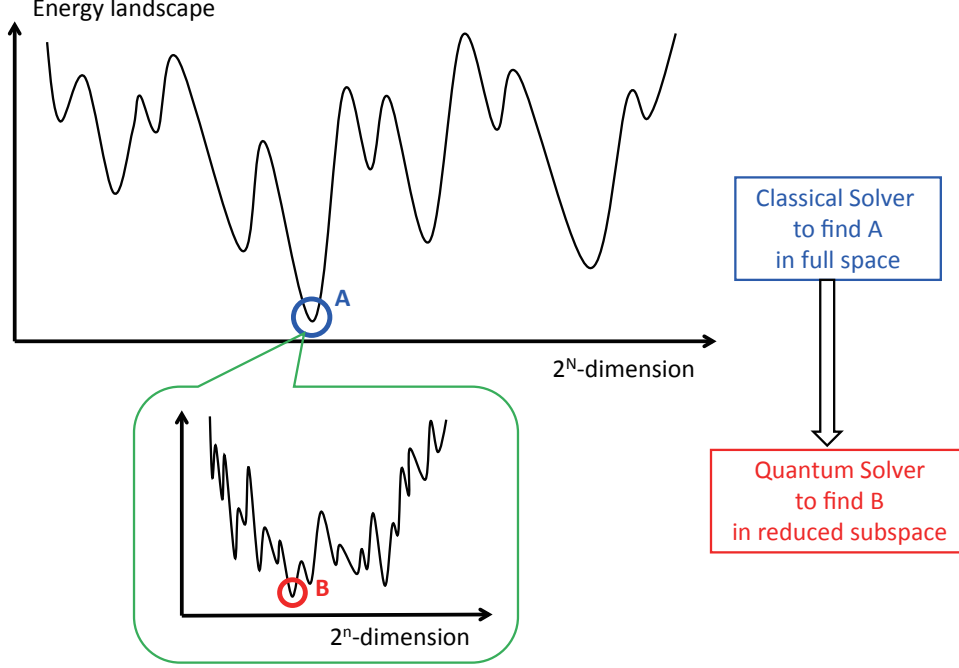


Figure 1: Concept of Hybrid Quantum Annealing (HQA) via Molecular Dynamics.

## Results

### Quantum annealing for spin variables

A large class of combinatorial optimization problems can be mapped onto the Ising model

$$\mathcal{H}_{\text{Ising}}(s) = \frac{1}{2} \sum_{i \neq j}^N J_{ij} s_i s_j + \sum_{i=1}^N h_i s_i, \quad (1)$$

with the Ising variables ( $\{s_i = \pm 1\}_{i=1}^N$ ), the symmetric coupling ( $J_{ij}$ ) and the external field ( $h_i$ ) [20]. The quantum annealing (QA) of transverse-field Ising model [2] provides an efficient method to solve the ground state of the system through the quantum deformation of  $\mathcal{H}_{\text{Ising}}$  as

$$\mathcal{H}_{\text{QA}}(\sigma; \tau) = A(\tau) \left[ - \sum_{i=1}^N \sigma_i^x \right] + B(\tau) \left[ \frac{1}{2} \sum_{i \neq j}^N J_{ij} \sigma_i^z \sigma_j^z + \sum_{i=1}^N h_i \sigma_i^z \right], \quad (2)$$

where  $\sigma_i^x, \sigma_i^z$  (and also  $\sigma_i^y$ ) are  $2 \times 2$  Pauli matrices at each site  $i$  ( $= 1, 2, \dots, N$ ), and  $\tau$  is a fictitious time taken to be in an interval  $[0, 1]$ . The scheduling functions  $A(\tau)$  and  $B(\tau)$  are chosen so that  $\mathcal{H}_{\text{QA}}(\tau)$  interpolates adiabatically the non-interacting spins with transverse field at initial time ( $A(0) \gg B(0)$ ) and the classical Ising spin-glass at final time ( $A(1) \ll B(1)$ ). (The actual scheduling functions in our numerical experiments below are  $A =$

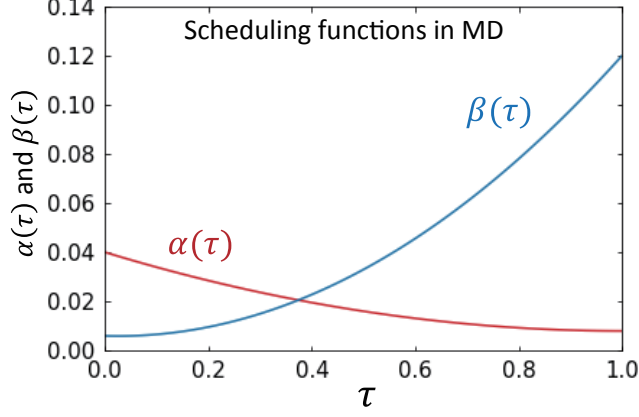


Figure 2: The actual scheduling functions in our MD run. See Methods section for their analytic forms.

$A_{\text{DW}}/2$  and  $B = B_{\text{DW}}/2$  where  $A_{\text{DW}}$  and  $B_{\text{DW}}$  are the scheduling functions given in Fig.2 of [21].) In the actual quantum annealing devices, quantum Ising spin is realized by the superconducting flux qubits described by a quantum Hamiltonian  $\mathcal{H}_{\text{device}}(\hat{\varphi}, \hat{p}; \tau)$  with the flux operators  $\hat{\varphi}_i$  and their conjugates  $\hat{p}_i$  with the canonical commutation,  $[\hat{\varphi}_j, \hat{p}_k] = i\hbar\delta_{jk}$  (see e.g. [22]).

### Molecular dynamics (MD) for flux variables

To construct a seamless hybrid between quantum and classical solvers, we introduce a classical Hamiltonian for flux variables as follows:

$$\mathcal{H}_{\text{MD}}(\varphi, p; \tau) = \alpha(\tau) \sum_{i=1}^N \left( \frac{p_i^2}{2} + V(\varphi_i) \right) + \beta(\tau) \left[ \frac{1}{2} \sum_{i \neq j}^N J_{ij} \varphi_i \varphi_j + \sum_{i=1}^N h_i |\varphi_i| \varphi_i \right], \quad (3)$$

where “MD” stands for the Molecular Dynamics,  $\{\varphi_i\}_{i=1}^N$  ( $\{p_i\}_{i=1}^N$ ) are the continuous flux variables (continuous conjugate momenta) which are classical counter parts of  $\{\hat{\varphi}_i\}_{i=1}^N$  ( $\{\hat{p}_i\}_{i=1}^N$ ). The MD evolution is parametrized by  $\tau = t/t_f \in [0, 1]$  with  $t \in [0, t_f]$  being the actual evolution time. The potential term  $V(\varphi)$  is a convex downward function of the form  $V(\varphi) = \varphi^M$  ( $M = 4, 6, 8, \dots$ ). Shown in Fig. 2 are the actual scheduling functions ( $\alpha(\tau)$  and  $\beta(\tau)$ ) to be used in the present paper. (The analytic forms are given in the [Methods section](#).)

It is in order here to discuss the basic properties of the above classical Hamiltonian: The term proportional to  $\alpha(\tau)$  in Eq.(3) ensures that each classical flux variable oscillates around  $\varphi_i = 0$  in early times. It plays a similar role as the transverse-field term proportional to  $A(\tau)$  in Eq.(2) which drives each spin state in early times to be an equal superposition of up and down. The term proportional to  $\beta(\tau)$  in Eq.(3) is a direct analogue of the Ising model: By decomposing the flux variables as  $\varphi_i = |\varphi_i| \text{sgn}(\varphi_i)$ , one finds the “correspondence” between the terms in Eq.(2) and Eq.(3);  $B J_{ij} \leftrightarrow \beta J_{ij} |\varphi_i \varphi_j|$  and  $B h_i \leftrightarrow \beta h_i |\varphi_i \varphi_i|$ . We note that the classical dynamical system achieves a faithful

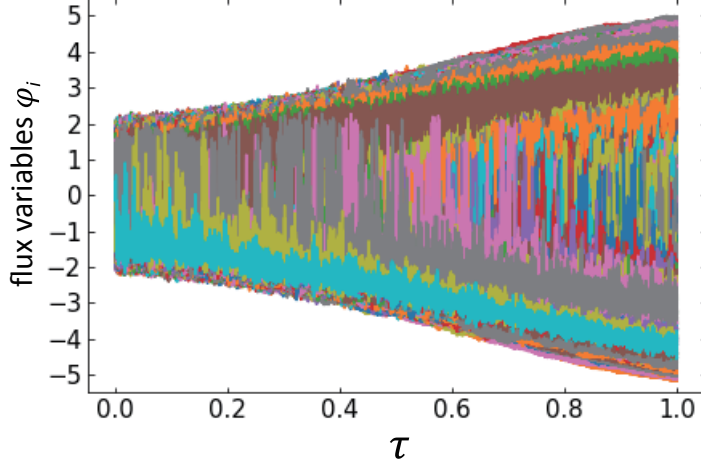


Figure 3: Trajectories of all flux variables  $\{\varphi_i\}_{i=1}^N$  for a typical Ising spin-glass model with  $N = 10,000$  and  $(\delta\tau)^{-1} = 50,000$ .

representation of the Ising model, only when all  $|\varphi_i|$  are frozen to a positive constant  $\mu$  and the equality  $B = \beta\mu^2$  gets satisfied. However, this cannot be achieved even for ideal MD solvers, and this is a generic problem of all classical solvers using Hamiltonian dynamics. On the other hand, our MD solver plays a role of a preconditioner for the quantum annealing, so that  $\varphi_i$ 's need not to settle down to  $\pm\mu$ . This is also the reason why  $\alpha(\tau = 1)$  can be non-zero as shown in Fig.2.

The Hamilton equations for the time evolution of the flux variables reads

$$g \frac{d\varphi_i}{d\tau} = \frac{\partial \mathcal{H}_{\text{MD}}(\varphi, p; \tau)}{\partial p_i}, \quad g \frac{dp_i}{d\tau} = -\frac{\partial \mathcal{H}_{\text{MD}}(\varphi, p; \tau)}{\partial \varphi_i}, \quad (4)$$

where  $\tau = t/t_f \equiv gt$ . The motion of the flux variables becomes adiabatic for  $g \rightarrow 0$ . We solve the above equations by the leapfrog algorithm ([Methods section](#)) on a GPGPU machine. As the initial conditions, we take  $\varphi_i(\tau = 0) = 0$ , with  $p_i(\tau = 0)$  randomly chosen to be  $+1$  or  $-1$ . As for the convex potential, we have tested  $M = 4, 6, 8$  and found that  $M = 6$  shows the best performance in terms of the evolution time and the achieved accuracy, so that we use this value throughout this paper.

### Sorting frozen and ambivalent variables

Shown in Fig.3 are all trajectories  $\{\varphi_i\}_{i=1}^N$  ( $N = 10,000$ ) as a function of  $\tau$  in a test MD evolution with a single set of Ising spin-glass parameters picked up randomly in the intervals,  $-1 \leq J_{ij} \leq +1$  and  $-2 \leq h_i \leq +2$ . The MD time step  $\delta\tau$  is chosen to be  $1/50,000$ . Moreover, we make an identification,  $g = \delta\tau$ , so that the small time step corresponds to the adiabatic evolution. Although there is a tendency that  $\varphi_i$  fall into two categories with positive sign and negative sign, we need to quantitatively separate the frozen variables and ambivalent variables. For that purpose, let us introduce time-

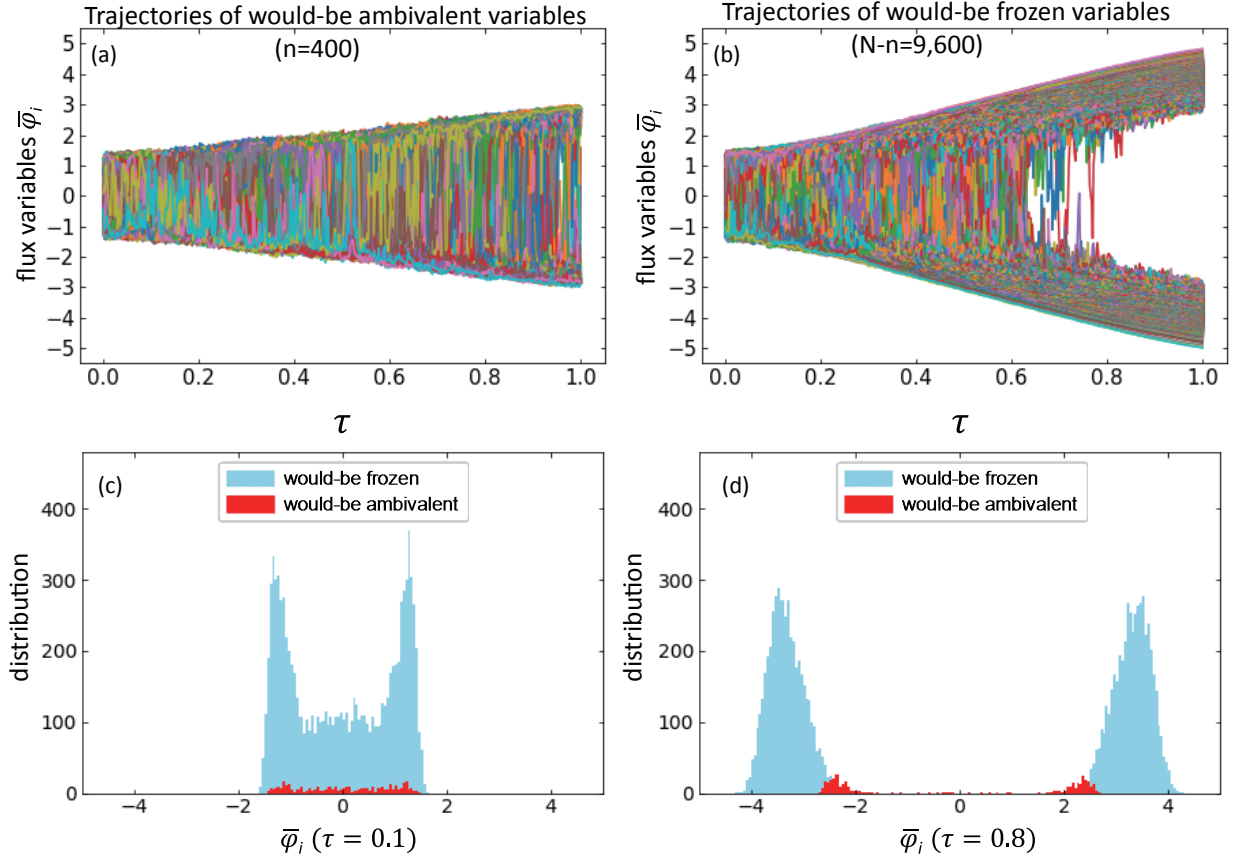


Figure 4: (a) Trajectories of would-be ambivalent variables  $\bar{\varphi}_{i'}$  with  $i' = 1, 2, \dots, n$ . (b) Trajectories of would-be frozen variables  $\bar{\varphi}_{i'}$  with  $i' = n + 1, \dots, N$ . Here,  $n$  and  $N$  are taken to be 400 and 10,000, respectively. Distributions of would-be frozen and ambivalent variables at  $\tau = 0.1$  (c) and at  $\tau = 0.8$  (d).

averaged flux variables,

$$\bar{\varphi}_i(\tau) \equiv \frac{1}{\delta} \int_{\tau-\delta}^{\tau} d\tau' \varphi_i(\tau'), \quad (5)$$

where the interval  $\delta$  should be sufficiently larger than  $\delta\tau$  and sufficiently smaller than 1. Then all trajectories can be sorted by using their magnitudes at  $\tau = 1$  as  $|\bar{\varphi}_{1'}(\tau = 1)| \leq |\bar{\varphi}_{2'}(\tau = 1)| \leq \dots \leq |\bar{\varphi}_{N'}(\tau = 1)|$  where  $i'$  is an index after sorting. Shown in Fig.4(a) with  $\delta = 100 \cdot \delta\tau$  are the low-lying trajectories  $\bar{\varphi}_{i'}(\tau)$  corresponding to  $i' = 1, 2, \dots, n$  with  $n = 400$ , while Fig.4(b) shows all the other 9,600 trajectories. These figures indicate that most of the flux variables are frozen in sign after the MD evolution, while small number of ambivalent variables remains at  $\tau = 1$ . In Fig.4(c) and (d), we show the distributions of the would-be frozen and ambivalent variables at an early time ( $\tau = 0.1$ ) and at a late time ( $\tau = 0.8$ ). As the time goes by, the distinction between two categories becomes prominent.

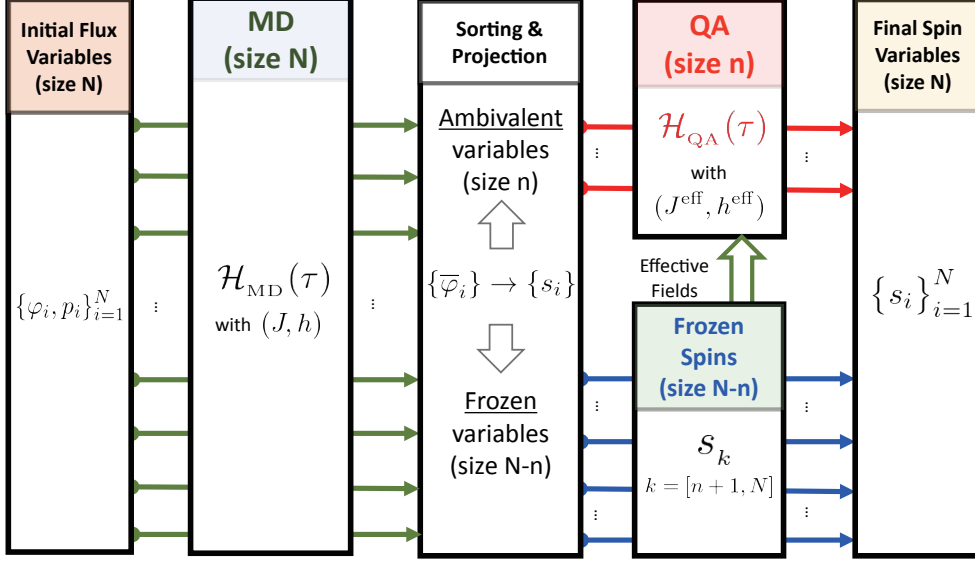


Figure 5: Flowchart of the Hybrid Quantum Annealing (HQA) via Molecular Dynamics (MD).

### Hybrid Quantum Annealing (HQA) via MD

Although our MD evolution combined with the above sorting algorithm can extract the ambivalent variables, it is extremely inefficient to continue the MD evolution toward  $\alpha = 0$  for sign of variables to settle down. Our approach to circumvent this issue is a novel hybrid scheme (HQA) where MD is used as a powerful preconditioner for QA. Currently available quantum annealers are still limited in size and accuracy. Nevertheless, as will be demonstrated below, the HQA can be a promising candidate to solve large  $N$  optimization problems in the future.

Our HQA is operated in the following way: We fix the frozen spins ( $k' = n+1, \dots, N$ ) by the projection  $s_{k'} = \text{sgn}(\bar{\varphi}_{k'}(\tau = 1))$ , while the ambivalent spins ( $i' = 1, \dots, n$ ) are sent to a reduced size Ising subsystem with the Hamiltonian,

$$\mathcal{H}'_{\text{Ising}}(s) = \frac{1}{2} \sum_{i' \neq j'}^n J_{i'j'}^{\text{eff}} s_{i'} s_{j'} + \sum_{i'=1}^n h_{i'}^{\text{eff}} s_{i'} \equiv \mathcal{H}_{\text{Ising}}(s | s_{k'=n+1, \dots, N} : \text{frozen}) - (\text{const.}). \quad (6)$$

Here the effective couplings read

$$J_{i'j'}^{\text{eff}} = J_{i'j'}, \quad h_{i'}^{\text{eff}} = h_{i'} + \sum_{k'=n+1}^N J_{i'k'} s_{k'}, \quad (i', j' = 1, 2, \dots, n). \quad (7)$$

This small subsystem of  $n$  degrees of freedom can be solved by embedding it into a quantum annealer. Shown in Fig.5 is an overall flowchart of our HQA starting from initial flux variables  $\{\varphi_i, p_i\}_{i=1}^N$  and ending with the final Ising-spin variables  $\{s_i\}_{i=1}^N$ .

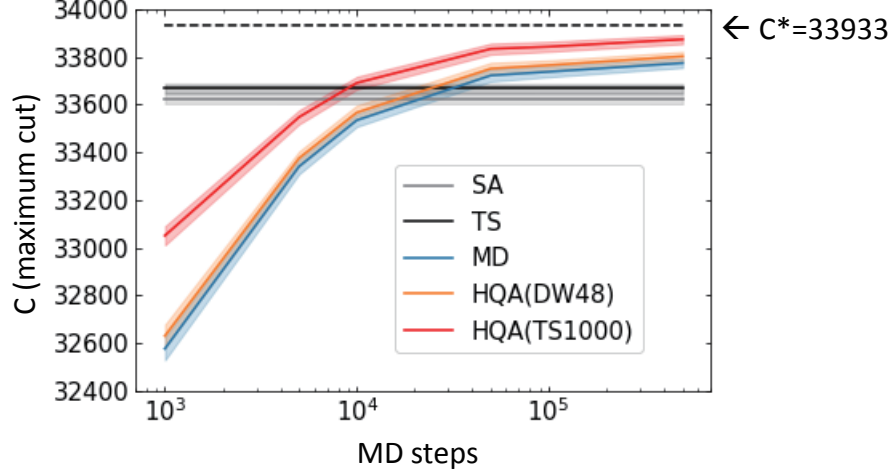


Figure 6: The maximum cut  $C$  in the MAX-CUT problem on a complete graph with 2000-node ( $K_{2000}$ ) obtained by different solvers. Theoretical estimate of the maximum cut is  $C^* = 33,933$ .

### HQA for MAX-CUT problem

To demonstrate how our HQA works, let us consider the MAX-CUT problem which is to find the size of the maximum cut ( $C$ ) in a given undirected graph. We take an all-to-all connected graph with 2000-node ( $K_{2000}$ ) having the random bimodal edge-weight  $w_{ij} = \pm 1$  with zero-mean. This problem has been used for benchmarking of various classical solvers including CIM [18] and SBM [19]. Mapping this problem into the Ising model (Methods section) with  $J_{ij} = w_{ij}$ ,  $h_i = 0$  and  $N = 2000$ , we compare the performance of three different solvers; our MD solver alone, HQA(DW48) which is an HQA with the  $n = 48$  subsystem solved by the D-Wave machine (DW\_2000Q\_5 [21]), and HQA(TS1000) which is an HQA with the  $n = 1000$  subsystem solved by the classical tabu search (TS) [23]. Due to the limited number of qubits in DW\_2000Q\_5, we can go only up to  $n = 48$  for QA. This is why we replaced DW by TS for the  $n = 1,000$  case anticipating that  $n \gg 48$  would be handled in the future QA machines. As reference classical solvers, we consider the tabu search (QBSolv [23]) and the simulated annealing (dwave.neal [24]).

In Fig.6, the horizontal axis represents the number of computational steps in MD  $(\delta\tau)^{-1}$ , while the vertical axis is the number of maximum cut ( $C$ ) obtained by different solvers. Colored solid curves are the results of different solvers, MD, HQA(DW48) and HQA(TS1000). The result of reference classical solvers with their default parameter settings for simulated annealing (SA) and for tabu search (TS) are shown by the gray straight line and the black solid line, respectively. The band associated with each line represents  $\pm 1\sigma$  confidence interval for 100 instances. (In actual numerical experiments, each  $J_{ij}$  is combined with a mirror instance  $-J_{ij}$  to ensure  $C_0 \equiv \frac{1}{4} \sum_{i \neq j} J_{ij} = 0$ .) Theoretical estimate of  $C$  using the finite size scaling analysis in statistical mechanics is  $C^* = -E^*/2 \simeq 33933$  [25] (Methods section) as shown by the dashed line. Here  $E^*$  is the ground-state energy of the Ising model averaged over instances.



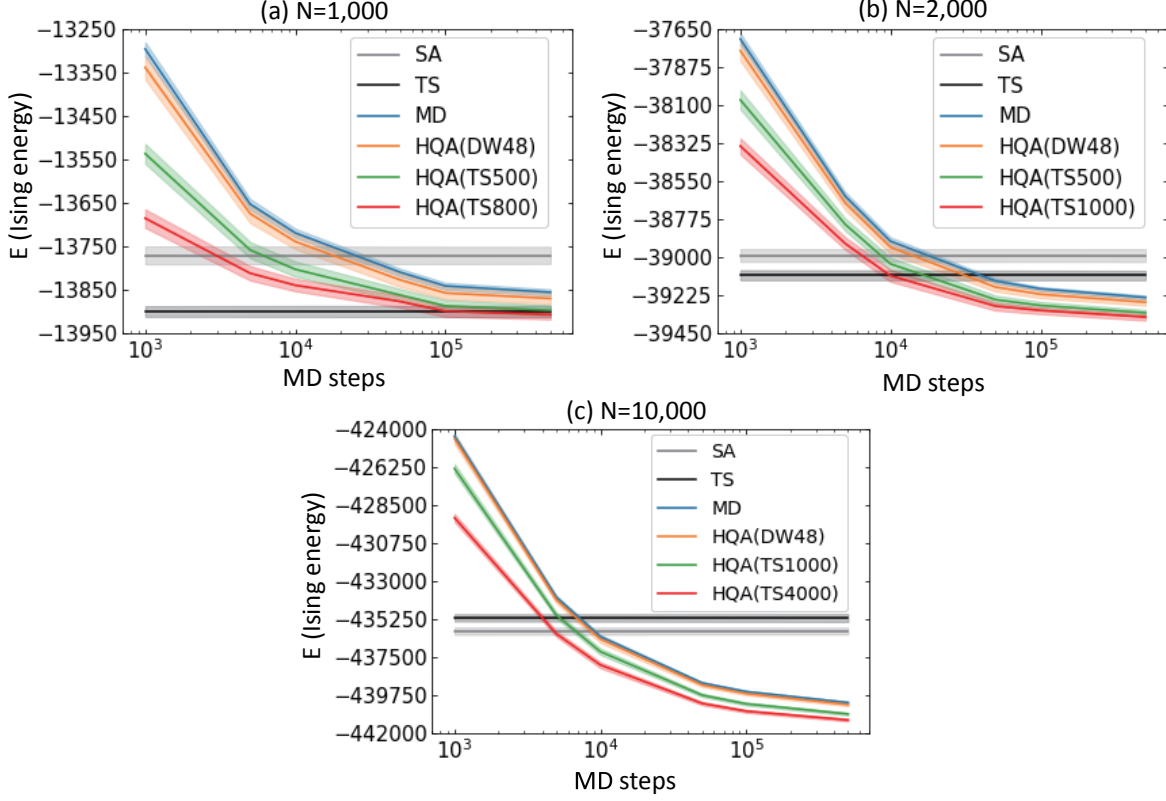


Figure 7: Results of the Ising energy  $E$  for the Ising spin-glass problem averaged over 100 instances by using different solvers with three different system sizes (a)  $N = 1,000$ , (b)  $N = 2,000$ , and (c)  $N = 10,000$ .

From the figure, one finds that the MD alone reaches up to 0.4 % deviation from  $C^*$  after 500,000 MD steps. This is more accurate than the results of other classical solvers such as SA (1% deviation) and TS (0.8 % deviation) obtained with their default settings. Moreover, HQA shows further improvement of the solution toward  $C^*$ : HQA(DW48) and HQA(TS1000) reach up to 0.3% and 0.2% accuracy, respectively. Although the latter is classical-classical hybrid, the trend to improve the accuracy as  $n$  increases is a promising sign for the future quantum-classical hybrid for large  $N$  problems.

### HQA for Ising spin-glass problem

Finally we consider a general Ising spin-glass model with 100 instances whose parameters  $J_{ij}$  and  $h_i$  are randomly chosen in the interval  $-1 \leq J_{ij} \leq +1$  and  $-2 \leq h_i \leq +2$ . Total system sizes are taken to be  $N = 1,000, 2,000$ , and  $10,000$  for several different values of  $n$  in Fig. 7(a,b,c). Results of the Ising energy averaged over instances  $E \equiv \langle \mathcal{H}_{\text{Ising}}^{(\min)}(s) \rangle$  are plotted as a function of the MD steps  $(\delta\tau)^{-1}$  ranging from 1,000 to 500,000. The colored solid curves are obtained by MD, HQA(DW48), HQA(TS500), HQA(TS800), HQA(TS1000) and HQA(TS4000), while the gray and black lines are the results of SA

and TS, respectively, with their default parameter settings. The band associated with each line represents  $\pm 1\sigma$  confidence interval for 100 instances.

The figures indicate that our MD provides already good accuracy to obtain the ground-state energy. Moreover, the performance of MD becomes better as the system size  $N$  increases in comparison to other classical solvers. Also, HQA shows further improvement (decrease of the energy) as in the case of the MAX-CUT problem: The trend to improve the accuracy is again a promising sign for large  $N$  problems when HQA(TS“n”) is replaced by HQA(DW“n”) in the future.

## Discussion

In this paper, we introduced a quantum-classical hybrid scheme (HQA) which utilizes the molecular dynamics as a preconditioner for quantum annealing. By taking a classical Hamiltonian for flux variables associated with spin variables, we have demonstrated that our HQA can solve combinatorial optimization problems with high accuracy. Moreover, our HQA shows better performance as the system size becomes larger. There are various interesting questions to be studied further. Among others, generalization of HQA with non-stoquastic interactions needs to be developed e.g. by adding off-diagonal kinetic terms in the MD solver,  $\sum_{i<j} \ell_{ij} p_i p_j$  [26]. Moreover, it is important to find proper classical dynamics applicable not only to the  $\mathbb{Z}_2$  spin variable but also to the binary (0 and 1) and multi-valued variables. Also, the algorithmic difference between our HQA (which preserves the adiabaticity from the beginning to the end) and SBM [19] (which breaks the adiabaticity at the point of bifurcation) should be clarified to understand the role of classical adiabaticity. With all these future works, our quantum-classical hybrid scheme provides a promising method to obtain efficient and precise solutions for optimization problems in science and technology.

## Methods

### Quantum annealing processor

The processor utilized in our numerical experiments is the lower-noise D-Wave 2000Q quantum processor DW\_2000Q\_5. The scheduling functions and the working graph of this processor is available in [21]. It enables us to embed the 48-node complete graph  $K_{48}$  to this processor with the standard triangle clique embedding scheme (See e.g. [27]). Quantum annealing is conducted with `chain_strength = 15`, `num_reads = 10,000`, `postprocess = 'optimization'`, and `annealing_time = 20` [ $\mu\text{sec}$ ].

### Scheduling functions for MD

We employ  $\alpha(\tau) = \alpha_f(\tau + \rho_1(1-\tau) + \rho_2\tau(\tau-1))$  and  $\beta(\tau) = \beta_f(\tau + \kappa_1(1-\tau) + \kappa_2\tau(\tau-1))$ ,

with  $(\alpha_f, \rho_1, \rho_2) = (0.008, 4, 3)$  and  $(\beta_f, \kappa_1, \kappa_2) = (0.12, 0.05, 1)$ . In early times when  $\alpha(\tau) \gg \beta(\tau)$ , the flux variables  $\{\varphi_i\}_{i=1}^N$  oscillate around  $\varphi_i = 0$ . This is a classical analogue of the initial quantum-superposition state of quantum annealing. If the motion of the flux variables is sufficiently faster than the evolution of scheduling functions, the system approaches adiabatically to the final state where most of the flux variables  $\{\varphi_i\}_{i=1}^N$  tend to be localized.

### Leapfrog algorithm

The Hamilton equations in Eq.(4) for  $i = 1, \dots, N$  can be solved accurately by the leapfrog algorithm [28]. With a given initial condition at  $\tau = 0$ ,  $\{\varphi_i(0), p_i(0)\}$ , we integrate the Hamilton equations with the step size  $\delta\tau$  being identified with  $g$  as follows:

$$\begin{cases} p_i^{(m+\frac{3}{2})} - p_i^{(m+\frac{1}{2})} &= -\alpha^{(m+1)} \frac{\partial V(\varphi)}{\partial \varphi_i} \Big|^{(m+1)} - 2\beta^{(m+1)} \left[ \frac{1}{2} \sum_{j=1}^N J_{ij} \varphi_j^{(m+1)} + h_i |\varphi_i^{(m+1)}| \right], \\ \varphi_i^{(m+2)} - \varphi_i^{(m+1)} &= \alpha^{(m+\frac{3}{2})} p_i^{(m+\frac{3}{2})}, \end{cases}$$

together with the initial half step,  $p_i^{(\frac{1}{2})} = p_i^{(0)} - \frac{\alpha^{(0)}}{2} \frac{\partial V(\varphi)}{\partial \varphi_i} \Big|^{(0)} - \beta^{(0)} \left[ \frac{1}{2} \sum_{j=1}^N J_{ij} \varphi_j^{(0)} + h_i |\varphi_i^{(0)}| \right]$  and  $\varphi_i^{(1)} = \varphi_i^{(0)} + \alpha^{(\frac{1}{2})} p_i^{(\frac{1}{2})}$ . Here  $m$  denotes the temporal step with  $\tau = m \cdot \delta\tau$  ( $m = 0, 1, 2, \dots$ ). Also, we introduced an abbreviated notation,  $f_i^{(m)} \equiv f_i(m \cdot \delta\tau)$  and  $f_i^{(m+\frac{1}{2})} \equiv f_i((m+\frac{1}{2}) \cdot \delta\tau)$  with  $f = \varphi, p, \alpha$  and  $\beta$ . The leapfrog integrator has only  $O((\delta\tau)^2)$  error and is essential for our MD evolution to be accurate enough. (If the Hamiltonian does not have explicit  $\tau$ -dependence which is not the case in the present situation, this integrator has nicer properties such as the time-reversibility and the symplectic property.)

**MAX-CUT and Ising spin-glass.** For a given undirected graph  $\mathcal{G} = (\mathcal{V}, \mathcal{E})$  with an edge-weight  $\{w_{ij}\}_{(ij) \in \mathcal{E}}$ , the MAX-CUT is a problem of finding a partition of vertices,  $\mathcal{V} = \mathcal{V}_+ \cup \mathcal{V}_-$  with  $\mathcal{V}_+ \cap \mathcal{V}_- = \emptyset$ , which maximizes the sum of  $w_{ij}$  connecting the two sets,  $C \equiv \sum_{i \in \mathcal{V}_+, j \in \mathcal{V}_-, (ij) \in \mathcal{E}} w_{ij}$ . This can be mapped to the problem of maximizing  $C(s) = \frac{1}{2} \sum_{(ij) \in \mathcal{E}} w_{ij} (1 - s_i s_j)$  with respect to the Ising spin variables  $s_i = \pm 1$ . One can rewrite  $C(s)$  in terms of the Ising spin-glass model ( $J_{ij} = w_{ij}$ ,  $h_i = 0$ ) as  $C(s) = -\frac{1}{2} \mathcal{H}_{\text{Ising}}(s) + C_0$ , with  $\mathcal{H}_{\text{Ising}}(s) = \frac{1}{2} \sum_{i \neq j} J_{ij} s_i s_j$  and  $C_0 \equiv \frac{1}{4} \sum_{i \neq j} J_{ij}$ . Minimizing the Ising energy  $\mathcal{H}_{\text{Ising}}(s)$  corresponds to maximizing the cut configuration. The instances of our experiment are given on the 2000-node complete graph  $K_{2000}$  with randomly generated bimodal weights  $J_{ij} = \pm 1$ . Therefore, the constant  $C_0$  follows the normal distribution with zero-mean for large  $N$ . The ground-state energy averaged over instances,  $E^* \equiv \langle \mathcal{H}_{\text{Ising}}^{(\min)}(s) \rangle$  for the corresponding spin-glass model has been discussed in [25]: The finite-size scaling implies  $E^*/N^{\frac{3}{2}} \xrightarrow{N \rightarrow \infty} e_0 + A/N^\omega$ . Here  $e_0 = -0.7631667265(6)$  is the Parisi energy [29], while  $\omega = 2/3$  and  $A = 0.70(1)$  are a conjectured value and a fitted value, respectively, of the numerical data for finite  $N$ . Combining all, the estimated value of the maximum-cut  $C^*$  on  $K_{2000}$  reads  $C^* \equiv -E^*/2 = 33933(4)$ , which we refer in Fig.6.

## References

- [1] F. Barahona, "On the computational complexity of Ising spin glass models," *Journal of Physics A* **15** (1982) 3241.
- [2] T. Kadowaki, H. Nishimori, "Quantum Annealing in the Transverse Ising Model," *Phys. Rev. E* **58** (1998) 5355-5363 [arXiv:cond-mat/9804280 [cond-mat.stat-mech]].
- [3] S Morita, H. Nishimori, "Mathematical foundation of quantum annealing", *J. Math. Phys.* **49** (2008)125210 [arXiv:0806.1859 [quant-ph]].
- [4] E. Farhi, J. Goldstone, S. Gutmann, J. Lapan, A. Lundgren, D. Preda, "A Quantum Adiabatic Evolution Algorithm Applied to Random Instances of an NP-Complete Problem", *Science* **292** (2001) pp. 472-475.
- [5] D. Aharonov, W. van Dam, J. Kempe, Z. Landau, S. Lloyd, and O. Regev, "Adiabatic Quantum Computation Is Equivalent to Standard Quantum Computation", *SIAM Rev.* **50** (2008).
- [6] M. W. Johnson, M. H. S. Amin, S. Gildert, T. Lanting, F. Hamze, N. Dickson, R. Harris, A. J. Berkley, J. Johansson, P. Bunyk, E. M. Chapple, C. Enderud, J. P. Hilton, K. Karimi, E. Ladizinsky, N. Ladizinsky, T. Oh, I. Perminov, C. Rich, M. C. Thom, E. Tolkacheva, C. J. S. Truncik, S. Uchaikin, J. Wang, B. Wilson, G. Rose, "Quantum annealing with manufactured spins," *Nature* **473** (2011) pp. 194-198
- [7] P. Hauke, H. G. Katzgraber, W. Lechner, H. Nishimori, W. D. Oliver, "Perspectives of quantum annealing: Methods and implementations", arXiv:1903.06559 [quant-ph].
- [8] T. Albash and D. A. Lidar, "Adiabatic quantum computation", *Rev. Mod. Phys.* **90** (2018) 015002.
- [9] J. Preskill, "Quantum Computing in the NISQ era and beyond," *Quantum* **2** (2018) 79.
- [10] M. Booth, S. P. Reinhardt, A. Roy, "Partitioning Optimization Problems for Hybrid Classical/Quantum Execution," D-Wave Technical Report Series 14-1006A-A, [available in <https://docs.ocean.dwavesys.com/projects/qbsolv/en/latest/index.html>].
- [11] S. Okada, M. Ohzeki, M. Terabe, S. Taguchi, "Improving solutions by embedding larger subproblems in a D-Wave quantum annealer," *Sci. Rep* **9**:2098 (2019) [<https://doi.org/10.1038/s41598-018-38388-4>].

- [12] N. Chancellor, “Modernizing Quantum Annealing using Local Searches,” *New Journal of Physics* **19** (2017) 023024 [arXiv:1606.06833 [quant-ph]].
- [13] H. Karimi, G. Rosenberg, H. G. Katzgraber, “Effective optimization using sample persistence: A case study on quantum annealers and various Monte Carlo optimization methods,” *Phys. Rev. E* **96** (2017) 043312 [arXiv:1706.07826 [cs.DM]].
- [14] J. King, M. Mohseni, W. Bernoudy, A. Fréchet, H. Sadeghi, S. V. Isakov, H. Neven, M. H. Amin, “Quantum-Assisted Genetic Algorithm,” arXiv:1907.00707 [quant-ph].
- [15] S. Feld, C. Roch, T. Gabor, C. Seidel, F. Neukart, I. Galter, W. Mauerer, C. Linnhoff-Popien, “A Hybrid Solution Method for the Capacitated Vehicle Routing Problem Using a Quantum Annealer,” *Front. ICT* **6**:13 (2019) [arXiv:1811.07403 [quant-ph]].
- [16] A. Ajagekar, T. S. Humble, F. You, “Quantum Computing Based Hybrid Solution Strategies for Large-scale Discrete-continuous Optimization Problems,” *Computers & Chemical Engineering*, **132** (2019) 106630 [arXiv:1910.13045[quant-ph]].
- [17] S. W. Shin, G. Smith, J. A. Smolin, U. Vazirani, “How “quantum” is the D-Wave machine?” arXiv:1401.7087 (2014).
- [18] H. Takesue, T. Inagaki, K. Inaba, T. Ikuta, T. Honjo, “A coherent Ising machine for 2000-node optimization problems”, *Science* **354** (2016) pp. 603-606. T. Inagaki et al., “Large-scale Coherent Ising Machine,” *J. Phys. Soc. Jpn.* **88** (2019) 061014.
- [19] H. Goto, K. Tatsumura, A. R. Dixon, “Combinatorial optimization by simulating adiabatic bifurcations in nonlinear Hamiltonian systems,” *Science Advances*, **5** eaav2372 (2019), pp.1-8.
- [20] A. Lucas, “Ising formulations of many NP problems,” *Front. Phys.* **2** (2014) pp. 1-5 [doi.org/10.3389/fphy.2014.00005].
- [21] ”QPU-Specific Physical Properties: DW\_2000Q\_5”, USER MANUAL (2019-08-07) [https://support.dwavesys.com/hc/article\\_attachments/360044041313/09-1210A-D-QPU-Properties\\_DW\\_2000Q\\_5.pdf](https://support.dwavesys.com/hc/article_attachments/360044041313/09-1210A-D-QPU-Properties_DW_2000Q_5.pdf)
- [22] R. Harris et al., “Experimental demonstration of a robust and scalable flux qubit,” *Phys. Rev.* **B81**, 134510 (2010).
- [23] `QBSolv` (version 0.2.10), available in <https://github.com/dwavesystems/qbsolv>
- [24] `dwave-neal` (version 0.5.1), available in <https://github.com/dwavesystems/dwave-neal>
- [25] S. Boettcher, “Simulations of ground state fluctuations in mean-field Ising spin glasses,” *J. Stat. Mech.* (2010) P07002; See also eLetter of [19] (28 April 2019), <https://advances.sciencemag.org/content/5/4/eaav2372/tab-e-letters>

- [26] I. Ozfidan et al., “Demonstration of nonstoquastic Hamiltonian in coupled superconducting flux qubits,” arXiv:1903.06139 [quant-ph]
- [27] T. Boothby, A. D. King, A. Roy, “Fast clique minor generation in Chimera qubit connectivity graphs,” *Quantum Inf Process* 15, 495-508 (2016). <https://doi.org/10.1007/s11128-015-1150-6>
- [28] J. Thijssen, “Computational Physics (2nd ed.)”, Cambridge University Press, London, (2013).
- [29] R. Oppermann, M. J. Schmidt, D. Sherrington, “Double criticality of the SK-model at  $T = 0$ ,” *Phys. Rev. Lett.* **98**, 127201 (2007). See also a review, M. Mezard, G. Parisi, M. Virasoro, “Spin Glass Theory and Beyond: An Introduction to the Replica Method and Its Applications,” *World Scientific Lecture Notes in Physics*: **9** (1986) pp.1-476

## Acknowledgments

The authors would like to thank Takashi Tsuboi for valuable comments and discussions. H.I. would also like to thank Tadashi Kadowaki and Akira Miki for valuable comments and discussions. T.H. was partially supported by the grants, JST CREST JPMJCR1913 and JSPS KAKENHI 19K22032. T.D. was partially supported by ”Priority Issue on Post-K computer” (Elucidation of the Fundamental Laws and Evolution of the Universe), ”Supercomputer Fugaku program” (Simulation for basic science: from fundamental laws of particles to creation of nuclei) and Joint Institute for Computational Fundamental Science (JICFuS).